Post-construction tensile load and strain behaviour of geogrids arranged in full-scale high walls

Kongkitkul, W.
Department of Civil Engineering, King Mongkut's University of Technology Thonburi, Thailand

Tatsuoka, F.
Department of Civil Engineering, Tokyo University of Science, Japan

Hirakawa, D.
Department of Civil and Environmental Engineering, National Defense Academy, Japan

Sugimoto, T.
Shizuoka Prefecture, Japan

Kawahata, S.
Nippon-koei Co., Ltd., Japan

Ito, M.
Maeda-Kosen Co., Ltd., Japan

Keywords: Creep, Rate-effect, Elasto-viscoplastic property, Geogrid, Reinforced-soil, Full-scale

ABSTRACT: Two high geogrid-reinforced soil (GRS) walls, 21.1-m high and 16.7 m-high, were constructed to support a taxi way of Mt. Fuji Shizuoka Airport, Japan, opened June 2009. To ensure small resilient and residual deformation and a high stability during severe earthquakes and heavy rainfalls during service, the backfill, which was well-graded gravelly soil, was well compacted while reinforced with geogrid layers. In the respective walls, a number of electric-resistant strain gages were attached to three geogrid layers to monitor geogrid tensile strains during and after wall construction. In-air tensile loading tests were performed on the geogrids to calibrate the readings of electric-resistant strain gauges against mechanically measured strains. After the end of wall construction, the geogrid tensile strains either increased at a very low rate or were kept essentially constant or noticeably decreased with time. The time histories of geogrid tensile forces were estimated from the measured time histories of geogrid strains by a non-linear three-component elasto-viscoplastic model using model parameters determined by the in-air tensile loading tests. The estimated tensile forces tend to decease with time at many locations or it is only at a very low rate when the geogrid forces tend to increase. It was estimated that, by the end of the prescribed life time (i.e., 50 years), the tensile force in the geogrid would be maintained substantially lower than the design working load and excessive deformation and creep rupture of the geogrid would be utterly unlikely in the two walls.

1 INTRODUCTION

Two high geosynthetic-reinforced soil (GRS) walls, 16.7-m high and 21.1-m high (walls 1 and 2), were constructed to support a taxi way of Mt. Fuji Shizuoka Airport in Shizuoka Prefecture in Japan which was opened to public June 2009 (Fig. 1, Fujinami et al. 2009). To ensure small deformation and a high stability during severe earthquakes and heavy rainfalls of the walls during service, well-graded gravelly soil retrieved from a nearby ancient river bed was selected as the backfill. As shown in Fig. 2, the backfill was compacted very well to an average degree of compaction higher than 95 % based on the maximum dry density obtained by compaction tests (modified Proctor).

In addition, tensile strains in three representative geogrid layers in the respective walls were continuously monitored during and after wall construction. The time histories of geogrid force were estimated from the measured time histories of geogrid strain, which were then extrapolated toward the end of a life time equal to 50 years. These analyses were performed by a non-linear three-component (NLTC) model that has been validated to be able to properly describe the rate-dependent tensile load-strain ($T-\varepsilon$) behaviour of a number of different geosynthetic reinforcement types (e.g. Hirakawa et al. 2003; Kongkitkul et al. 2004, 2007).

2 GEOGRIDS ARRANGED IN THE WALLS

The geogrid made of Aramid fibre coated with HDPE was used to reinforce the backfill. Seven different types having different design rupture strengths T_d ranging from 20 to 87 kN/m were used. These T_d values were obtained by reducing the fast loading tensile strengths of new products using a creep reduction factor equal to 1.6. The installation damage and durability reduction factors were confirmed to be equal to unity based on validation tests. The

Table 1 Strength properties of three representative geogrid types

Geogrid type	Ultimate tensile strength (kN/m)*	Design tensile strength T_d (kN/m)**	Layer No. (see Figs. 1a & b)	
			Wall 1	Wall 2
G-100	95	59	21	13
G-120	112	70	5	23
G-150	140	87	13	3

*: strain rate = 1.0 %/min

**: after applying creep reduction factor = 1.6; installation damage factor = 1.0; and durability reduction factor = 1.0

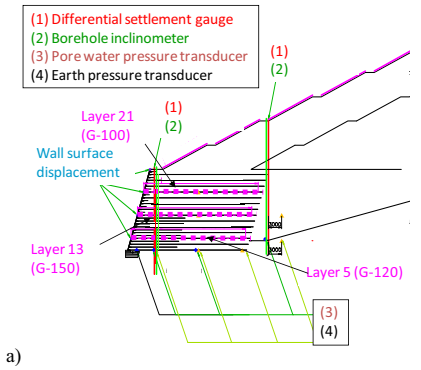

a)

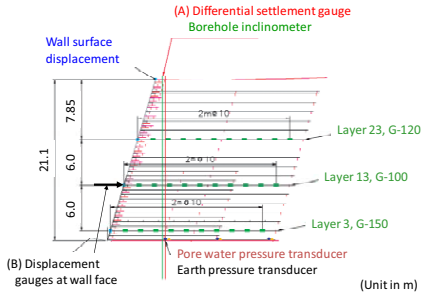

b)

Fig. 1 Typical cross-sections of: a) wall 1; and b) wall 2

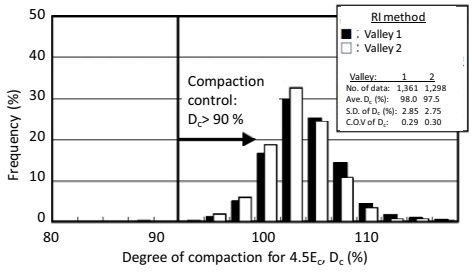

Fig. 2 Distributions of measured degrees of compaction of the backfill

properties of the three respective geogrid types on which electric-resistant strain gauges (SGs) were attached in the two walls are listed in Table 1. Ten to thirteen SGs were installed on each of three selected

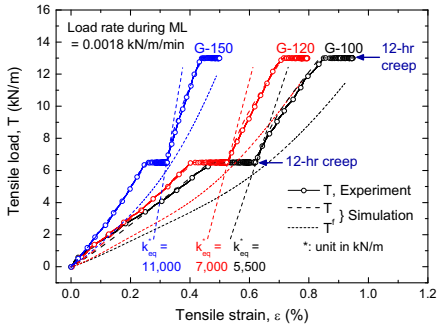

a)

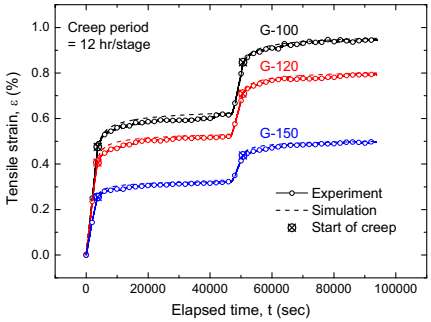

b)

Fig. 3 In-air tensile test results and model simulations: a) $T-\varepsilon$ relations; and b) time histories of ε

geogrid layers in the respective walls, geogrid layer Nos. 5, 13 and 21 in the wall 1 (Fig. 1a) and Nos. 3, 13 and 23 in the wall 2 (Fig. 1b).

Figs. 3a and 3b show the $T-\varepsilon$ relations and time histories of ε from unconventional load-controlled tensile loading tests on new products. In these tests, sustained loading tests were performed for 12 hours at two levels of T equal to 6.5 and 13 kN/m during otherwise monotonic loading (ML) at a load rate of 0.0018 (kN/m)/min. The simulations presented in these figures are explained later.

3 GEOGRID STRAINS IN THE WALLS

Figs. 4a, b and c show time histories of ε measured in geogrid layer Nos. 5 (G-120), 13 (G-150) and 21 (G-100) in wall 1. Figs. 5a, b and c show similar results in geogrid layer Nos. 3 (G-150), 13 (G-100) and 23 (G-120) in wall 2. The origin of elapsed time was defined when the respective geogrid layers were installed. Unlike wall 2, a 45-m high sloped embankment was constructed back of wall 1 for a period of about nine months starting about two months after the wall completion. It seems that the geogrid tensile strain somehow increased by the load from the sloped embankment. The following trends of behaviour may be seen from these figures:

1. In general, the increasing rate of ε is high during wall construction. The increase at a high rate stopped when the wall was completed.

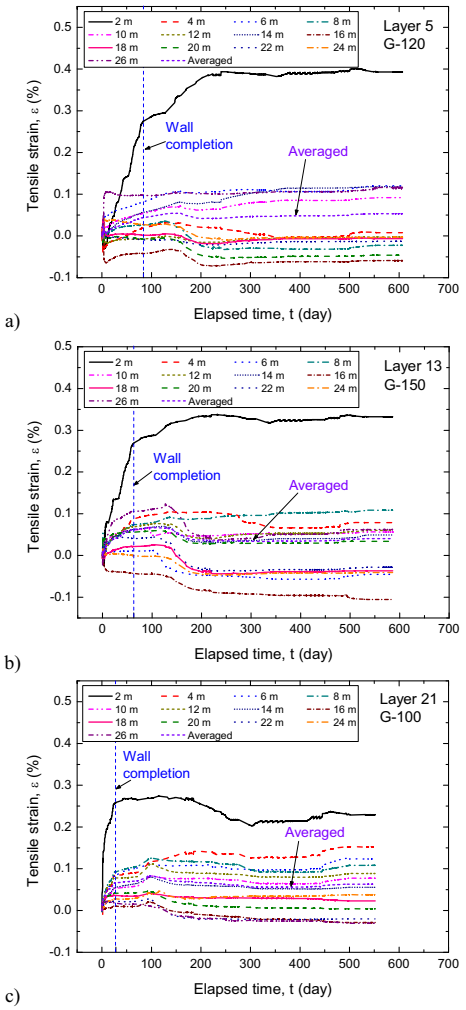

Fig. 4 Time histories of individual and average tensile strains in the three geogrid layers in wall 1: layer Nos. a) 5 (G-120); b) 13 (G-150); and c) 21 (G-100); the distances (in m) are back from wall face

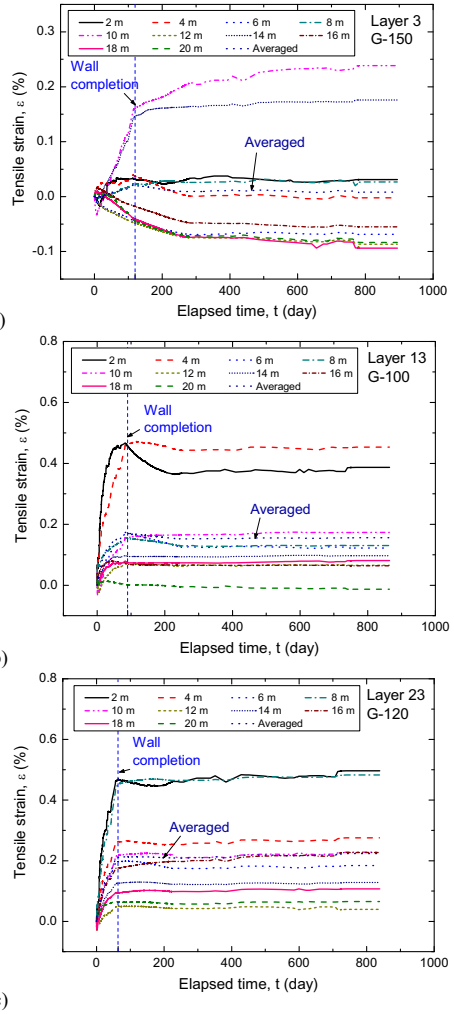

Fig. 5 Time histories of individual and average tensile strains of geogrid layers in wall 2: layer Nos. a) 3 (G-150); b) 13 (G-100); and c) 23 (G-120); the distances (in m) are back from wall face

2. The values of ε at the wall completion in the respective layers were largest mostly at 2 m back from the wall face. This indicates that there is no deep global potential failure plane indicating unstable global behaviour of these two walls.
3. After wall completion, the ε value continued increasing at some locations, but the increasing rate was very low. At other locations, the ε stopped increasing. At the other locations, the ε even started decreasing with time.
4. The largest observed ε values are substantially lower than the strain at rupture. Therefore, the T values obtained by substituting these strains into the $T-\varepsilon$ relations shown in Fig. 3a are substantially lower than the respective tensile rupture strengths, listed in Table 1.

4 MODELLING OF GEOGRID

Hirakawa et al. (2003) and Kongkitkul et al. (2004, 2007) showed that a NLTC model (Di Benedetto et al. 2002; Tatsuoka et al. 2002, 2008; Fig. 6) can simulate very accurately the rate-dependent $T-\varepsilon$ behaviours of many different types of geosynthetic reinforcement, as typically shown in Fig. 3. According to the model, T at a given irreversible strain ε^{ir} is obtained by adding the viscous component T^{v} to the inviscid component T^{f} at the same ε^{ir}, while the tensile strain rate $\dot{\varepsilon}$ by adding the elastic component $\dot{\varepsilon}^{e}$ to the irreversible component $\dot{\varepsilon}^{ir}$ at the same T. Kongkitkul et al. (2008) reported that the geogrid

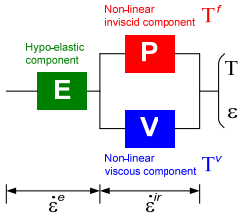

Fig. 6 Non-linear three-component model modified for polymeric geosynthetic reinforcement (Hirakawa et al. 2003; Kongkitkul et al. 2004, 2007)

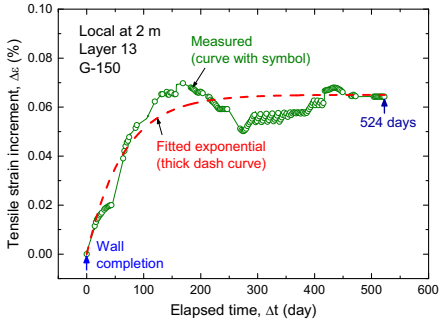

Fig. 7 Measured and fitted time histories of tensile strain increment of G-150 geogrid at 2 m back from the wall face in geogrid layer No. 13 of wall 1

made of Aramid fibre, used to construct these two walls, exhibited Isotach viscosity. In that case, T is obtained as:

$$\left[T\left(\varepsilon^{ir},\dot{\varepsilon}^{ir}\right)\right]_{(\varepsilon^c)} = \left\{1+g_v\left(\dot{\varepsilon}^{ir}\right)\right\}\cdot\left[T^f\left(\varepsilon^{ir}\right)\right]_{(\varepsilon^c)} \quad (1a)$$

$$g_v\left(\varepsilon^{ir}\right) = \alpha^*\cdot\left(\left|\dot{\varepsilon}^{ir}\right|/\dot{\varepsilon}_o^{ir}\right)^{1+b^*} \quad (1b)$$

where $g_v\left(\varepsilon^{ir}\right)$ is the viscosity function, which is a highly non-linear function of $\dot{\varepsilon}^{ir}$; and α^*, b^* and $\dot{\varepsilon}_o^{ir}$ are the material constants. By analysing the test results of this geogrid type by Hirakawa et al. (2003), the parameters: α^*= 0.18, b^*= -0.65 and $\dot{\varepsilon}_o^{ir}$= 10^{-6} %/s were obtained. It was found that these parameters are also relevant to the three types of geogrid where strains were measured in the two walls. Not only the $T-\varepsilon$ relations (Fig. 3a) but also the time histories of creep strain (Fig. 3b) are simulated very well by the NLTC model using these parameters.

5 ESTIMATION OF TENSILE FORCES

To obtain the time histories of geogrid tensile force by the NLTC model, the time histories of measured ε in the monitored geogrid layers were fitted by empirical equations. Fig. 7 shows the time history of ε defined zero at the wall completion at 2 m back from the wall face in geogrid layer No. 13 (G-150) in wall 1, which is typical of those that exhibited a continuous increase with time (Figs. 4 and 5). To alleviate difficulties in the subsequent analysis due to irregular variations with time in the time histories of ε, Eq. 2a was fitted to the data to obtain smooth time histories, as shown in Fig. 7:

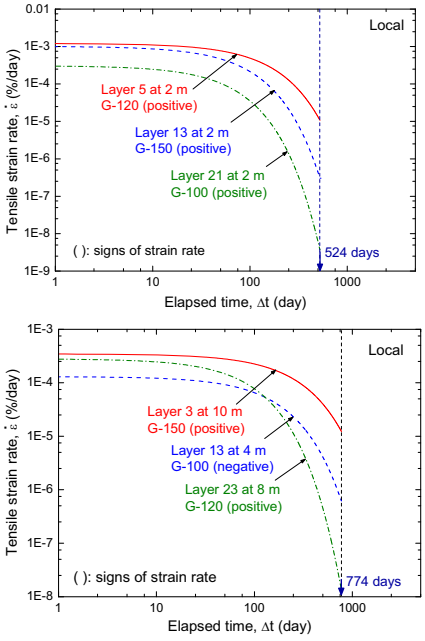

Fig. 8 Geogrid strain rate - elapsed time relations from the fitted time histories of tensile strain of geogrids at locally selected locations: a) wall 1; and b) wall 2

$$\Delta\varepsilon = A_1\cdot\left(1-e^{-\Delta t/t_1}\right)+A_2\cdot\left(1-e^{-\Delta t/t_2}\right) \quad (2a)$$

$$\dot{\varepsilon} = \frac{\partial\varepsilon}{\partial t} = \frac{A_1\cdot e^{-\Delta t/t_1}}{t_1}+\frac{A_2\cdot e^{-\Delta t/t_2}}{t_2} \quad (2b)$$

where A_1, A_2, t_1 and t_2 are constants. Eq. 2b is obtained by differentiating Eq. 2a with respect to time.

Figs. 8a and b show the time histories of tensile strain rate at the selected locations of the geogrid layers, where the maximum tensile strain was mobilised in respective geogrid layers, in walls 1 and 2 (Figs. 4 and 5). The strain rate at 4 m back from the wall face in geogrid layer No. 13 of wall 2 were negative, which means that the geogrid strain decreases with time. The time histories of tensile strain rate were extrapolated toward the end of 50 years (a design life typical for civil engineering structures).

Figs. 9a, b and c show the relationships between the estimated tensile force and the measured and fitted local tensile strain before and after the wall completion at selected locations in the three monitored geogrid layers in wall 1. Similarly, Figs. 10a, b and c show the local relations at selected locations in the three monitored geogrid layers in wall 2. The solid curves presented in Figs. 9 and 10 indicate the $T-\varepsilon$ relations from the origin (0,0), defined when the respective geogrid layers were installed, obtained from

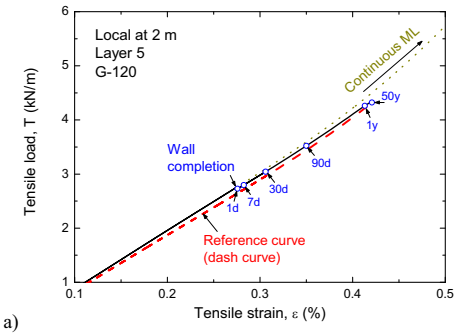

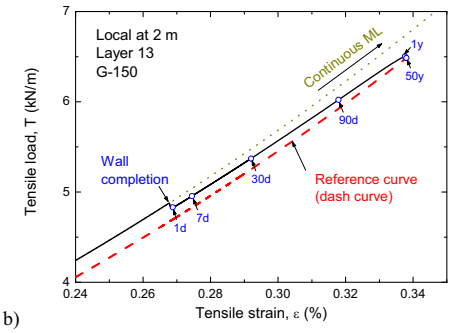

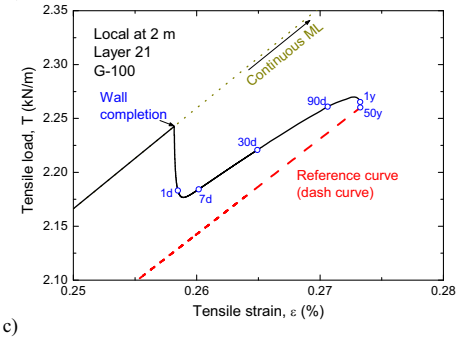

Fig. 9 Tensile load - local strain relations of geogrid at selected locations in wall 1, extrapolated to 50 years, in layer Nos.: a) 5 (G-120); b) 13 (G-150); and c) 21 (G-100)

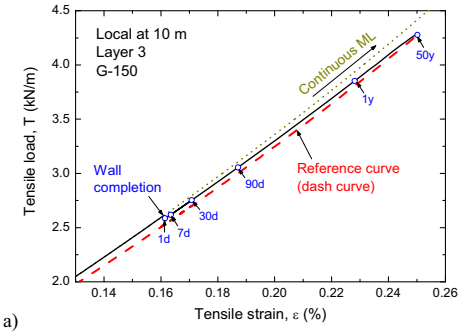

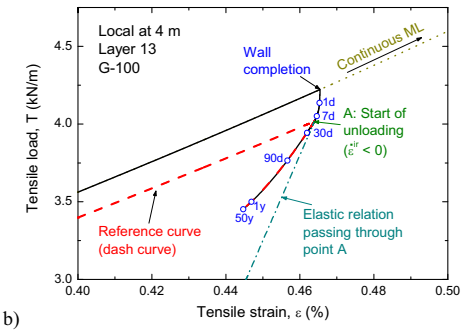

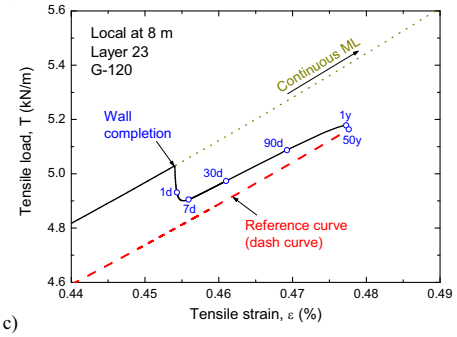

Fig. 10 Tensile load - local strain relations of geogrid at selected locations in wall 2, extrapolated to 50 years, in layer Nos.: a) 3 (G-150); b) 13 (G-100); and c) 23 (G-120)

the measured and fitted time histories of tensile strain extrapolated to 50 years. The dotted curves represent the relations if ML had still continued after the wall completion at the strain rate at the end of wall construction. In all the relations, immediately after the wall completion, the loading condition (where $\dot{\varepsilon}^{ir} > 0$) is maintained. Subsequently, in some cases, the loading condition continued by the end of 50 years. In geogrid layer No. 13, at 4 m back from the wall face (Fig. 10b), the neutral state (where $\dot{\varepsilon}^{ir} = 0$), which is located on the reference relation for loading, is reached. Then, the $\dot{\varepsilon}^{ir}$ becomes negative and the $T-\varepsilon$ behaviour enters into an unloading branch (where $\dot{\varepsilon}^{ir} < 0$).

Figs. 9a and b show the estimated $T-\varepsilon$ relations in the two cases where the geogrid is locally most severely loaded in those analysed in wall 1. Fig. 10a shows similar case in wall 2. In these cases, after the wall completion, the tensile strain continued increasing with time at such a relatively high rate as that the geogrid tensile force also continuously increased with time. Yet, the predicted tensile forces after 50 years are only about 4.32 and 6.49 kN/m respectively for geogrid layer Nos. 5 and 13 of wall 1 and about 4.25 kN/m for geogrid layer No. 3 of wall 2. These values are substantially lower than the respective design ultimate tensile strengths (Table 1).

6 DISCUSSIONS

With the two high geogrid-reinforced steep walls described above, it is very likely that the geogrid tensile force would be kept to values substantially

lower than the respective design ultimate tensile strengths by the end of the prescribed design life. Because of the above, the estimated increasing rate of geogrid tensile force was very low, or essentially zero, or even negative. This was due also to the fact that the stress (load) – strain behaviours of both geogrid and backfill are rate-dependent due to their viscous properties. In particular, the reduction of tensile strain with time in the geogrid is due likely to compressive creep strains that take place in the horizontal direction in the backfill caused by the tensile force in the reinforcement (Tatsuoka et al. 2004; Tatsuoka 2008). These observations and analyses presented above indicate that the possibility of excessive tensile deformation and tensile creep rupture of the geogrid arranged in these two walls by the end of the prescribed design life is extremely low.

7 CONCLUSIONS

The following conclusions can be derived from the performance of two high GRS walls constructed by highly compacting well-graded gravelly soil while providing an effective drainage system and geogrid layers installed in the walls and its analysis:

1. The increase in the geogrid strain after the end of wall construction is generally very small, or even a decrease was observed, in six monitored geogrid layers.
2. The geogrid tensile force estimated by a non-linear three-component model either increased at a very small rate, or even decreased with time. It was estimated that the geogrid tensile force would be kept to values substantially lower than the respective design ultimate tensile strengths by the end of design life (i.e., 50 years).
3. It is therefore utterly unlikely that excessive tensile deformation and tensile creep rupture of the geogrid take place by the end of design life in these two walls.

REFERENCES

Di Benedetto, H., Tatsuoka, F. & Ishihara, M. 2002. Time-dependent shear deformation characteristics of sand and their constitutive modelling. *Soils and Foundations*, Vol.42 (2), pp.1-22.

Fujinami, T., Sugimoto, T., Yamashita, D. & Kawahata, S. 2009. Application of geosynthetic-reinforced wall technology and backfill compaction control in constructing high embankment for Mt. Fuji Shizuoka Airport. *Monthly Journal Kiso-ko (Foundation Engineering and Equipment)*, Vol.37 (7), pp.92-95 (in Japanese).

Hirakawa, D., Kongkitkul, W., Tatsuoka, F. & Uchimura, T. 2003. Time-dependent stress-strain behaviour due to viscous properties of geogrid reinforcement. *Geosynthetics International*, Vol.10 (6), pp.176-199.

Kongkitkul, W., Hirakawa, D., Tatsuoka, F. & Uchimura, T. 2004. Viscous deformation of geosynthetic reinforcement under cyclic loading conditions and its model simulation. *Geosynthetics International*, Vol.11 (2), pp.73-99.

Kongkitkul, W., Hirakawa, D. & Tatsuoka, F. 2007. Viscous behaviour of geogrids; experiment and simulation. *Soils and Foundations*, Vol.47 (2), pp.265-283.

Kongkitkul, W., Hirakawa, D., Sugimoto, T., Kawahata, S., Yoshida, T., Ito, S. & Tatsuoka, F. 2008. Post-construction time history of tensile load in geogrid arranged in a full-scale high wall. *Proc. 4th Asian Regional Conference on Geosynthetics (GeoAsia 2008)*, Shanghai, China, 17 – 20 June 2008, Li, Chen & Tang (eds.), Zhejiang University Press & Springer, pp.64-69.

Tatsuoka, F. 2008. Geosynthetics engineering, combining two engineering disciplines. Keynote Lecture. *Proc. 4th Asian Regional Conference on Geosynthetics (GeoAsia 2008)*, Shanghai, China, 17 – 20 June 2008, Vol.2, pp. 1-35.

Tatsuoka, F., Ishihara, M., Di Benedetto, H. & Kuwano, R. 2002. Time-dependent shear deformation characteristics of geomaterials and their simulation. *Soils and Foundations*, Vol.42 (2), pp.103-129.

Tatsuoka, F., Hirakawa, D., Shinoda, M., Kongkitkul, W. & Uchimura,T. 2004. An old but new issue; viscous properties of polymer geosynthetic reinforcement and geosynthetic-reinforced soil structures. Keynote Lecture. *Proc. 3rd Asian Regional Conference on Geosynthetics (GeoAsia 2004)*, J.B. Shim, C. Yoo and H.-Y.Jeon (eds.), Seoul, pp.29-77.

Tatsuoka, F., Di Benedetto, H., Enomoto, T., Kawabe, S. & Kongkitkul, W. 2008. Various viscosity types of geomaterials in shear and their mathematical expression. *Soils and Foundations*, Vol.48 (1), pp. 41-60.